J Fluoresc (2009) 19:975–988
DOI 10.1007/s10895-009-0497-4

ORIGINAL PAPER

Thermodynamics of the Dimer Formation of $2^I,3^I$-*O*-(*o*-Xylylene)-per-*O*-Me-γ-cyclodextrin: Fluorescence, Molecular Mechanics and Molecular Dynamics

Maria José González-Álvarez · José Vicente · Carmen Ortiz Mellet · José Maria García Fernández · Francisco Mendicuti

Received: 8 January 2009 / Accepted: 5 June 2009 / Published online: 14 July 2009

Abstract The thermodynamics of the dimer formation of $2^I,3^I$-*O*-(*o*-xylylene)-per-*O*-Me-γ-cyclodextrin (X*m*γCD) in aqueous solution was studied by fluorescence techniques, Molecular Mechanics and Molecular Dynamics. Lifetime averages $\langle\tau\rangle$, obtained from fluorescence decay profiles upon excitation of the xylylene appended group, were used as the property sensitive to the association process. The dimerization equilibrium constants (K_D) were obtained from non-linear regression analysis of the plots of $\langle\tau\rangle$ against [X*m*γCD] at several temperatures and they were compared with the values obtained for the counterparts X*m*α- and X*m*βCDs. The van't Hoff plot allows us to obtain the ΔH and ΔS showing that the dimerization process was also entropically disfavoured. Molecular Mechanics as well as Molecular Dynamics calculations in the presence of water were also employed to study the conformational behaviour of isolated X*m*γCDs, the possible structure of the dimers formed and the driving forces involved in such association processes. Results indicate that those conformations where Xy moiety does not block the cavity entrance are favoured. Dimers are preferably formed by head-to-head CD approaching. However, the formation of stable head-to-tail is not dismissed.

Keywords Cyclodextrins · Xylylene derivatives · Fluorescence · Molecular mechanics · Molecular dynamics

M. J. González-Álvarez · F. Mendicuti (✉)
Dpto. Química Física, Universidad de Alcalá,
28871 Alcalá de Henares, Spain
e-mail: francisco.mendicuti@uah.es

J. Vicente · J. M. G. Fernández
Instituto de Investigaciones Químicas, CSIC,
41092 Sevilla, Spain

C. O. Mellet
Dpto. Química Orgánica, Facultad de Química,
Universidad de Sevilla,
41012 Sevilla, Spain

Introduction

Cyclodextrins (CDs) are cyclic oligosaccharides consisting of α(1→4)-linked D-glucopyranoside units that are widely used as hosts for molecule guests of appropriate shape and size that can undergo at least partial inclusion into their hollow cavities [1–4]. Complexation is usually accompanied by changes in the polarity and microviscosity surrounding the guest, thus modifying the spectroscopic properties when such guests contain a chromophore group [5–10]. Analogously, chemically modified CDs bearing covalently attached moieties (capped CDs) can undergo self-inclusion and self-association phenomena, depending on the size and shape of the appended group and the flexibility and length of the chain that connects it to the CD core. Both processes can be exploited to control the complexation of isolated guest molecules [11–56]. Self-inclusion or self-association also involves changes in the spectroscopic properties of CD-appended chromophore groups, which has found application in the design of chemo-sensors [12, 16, 19, 22, 24, 28, 38, 42, 52, 53] and light harvesting host molecules for photonic devices [13, 14, 17, 18, 29, 30, 47].

In most of the reported examples of capped CDs, the pendant chromophore group is linked to one or two primary C(6) positions [12, 16, 19, 21, 22, 24, 28, 31–33, 37, 38,

41–43, 46, 48–51, 53]. Examples of secondary-face fluorophore-appended CDs are rather limited [20, 23, 25, 39, 56]. A particularly interesting architecture is the case where a bidentate group is attached to two different secondary positions in the CD torus [57]. The mobility of the appended element must be then significantly restricted and, consequently, a deep change in the sensing abilities towards different guests is expected.

We recently described the synthesis and characterization of several $2^I,3^I$-*O*-(*o*-xylylene)-permethylated CDs, in which a xylylene group was bridging the vicinal O-2 and O-3 secondary positions of a glucopyranose unit through a bidentate-hinge [58]. Fluorescence, Molecular Mechanics (MM) and Molecular Dynamics (MD) techniques were used for studying the formation of dimeric aggregates from $2^I,3^I$-*O*-(*o*-xylylene)-per-*O*-Me-α- and -β-cyclodextrins (named X*m*αCD and X*m*βCD respectively) in water, corroborating preliminary dynamic ^{1}HNMR evidence [56, 58]. The fluorescence decay profiles of the xylylene moiety were fitted to the sum of three-exponential decays, two of which were ascribed to the monomer and dimer species and the third, shorter lived one to the scattering of the sample and stray light. The dimerization equilibrium constants (K_D) in the 5–45°C range, obtained from average lifetime variations with [X*m*CD], were similar and relatively low for both the α and βCD derivative (~180 M^{-1} and ~200 M^{-1} at 25°C, respectively). Dimerization processes were enthalpy-governed and entropy-disfavoured, with $\Delta H < 0$ values typical of attractive van der Waals and electrostatic type interactions and $\Delta S < 0$ values corresponding to the loss of degrees of rotational and translational freedom, which overcome the loss of solvation order during dimerization. MD calculations of X*m*CD monomers at different temperatures demonstrated the presence of an *open* ⇄ *capped* equilibrium which is noticeably displaced to the *open* conformation. In the *capped* conformation the *o*-xylylene group seems to partially block the secondary rim CD entrance. MM and MD in the presence of water reveal that the most stable dimers are formed when both X*m*CD approach head-to-head with both CDs placed in an *open* (*or half-open*) conformation. In these dimer structures the Xy groups are close enough to mutually interact and, although they do not penetrate inside the cavity of the neighbour CD, they are both relatively shielded from bulk water. The head-to-head dimer structure agrees with the analysis of the quenching results and those obtained from the study of the complexation of a α,α'-dimethoxy-*o*-xylene (*o*Xy) with permethylated α- and -β-cyclodextrins (*m*αCD and *m*βCD) and the heterodimerization of X*m*CDs with *m*αCD and *m*βCDs.

The present work extends the study of the aggregation in water of these systems to the larger-ring cyclooligosaccharide homologue $2^I,3^I$-*O*-(*o*-xylylene)-per-*O*-Me-γ-CD (X*m*γCD). Steady-state and time-resolved fluorescence spectroscopy measurements, as well as MM and MD calculations were performed. Aggregation number, association constant and thermodynamics parameters upon association were obtained. The complexation of *o*Xy and the hetero-association of X*m*γCD with *m*γCD respectively were also studied. Molecular Mechanics (MM) as well as Molecular Dynamics (MD) calculations in the vacuo and in the presence of water were employed to study the conformational behavior of the isolated X*m*γCD and the possible structures for the associated forms.

Materials and methods

Reagents and solution preparation

The synthesis and characterization of X*m*γCD and *m*γCD were described elsewhere [58]. α,α'-Dimethoxy-*o*-xylene (*oXy*), whose preparation was already described [59] was used as a model compound for the appended group. CD aqueous solutions (water deionized by Milli-Q system) were prepared by weight and they were stirred for at least ~24 h prior to measuring. X*m*γCD/water solutions were in the 0.586–13.897 mM concentration range. For studying the *oXy* (X*m*γCD) complexation (hetero-dimerization) with *m*γCD the *oXy* (X*m*γCD) concentration was kept constant and the [*m*γCD] was changed in the 0–8.94 mM (0–10.65 mM) range. The use of larger X*m*γCD (or *m*γCD) concentrations resulted in the appearance of a powdered precipitate. Nevertheless, all measurements were performed in transparent solutions. A characteristic of X*m*γCDs, already observed for methylated cyclodextrins [60] and for X*m*αCD and X*m*βCDs [58], is that the solubility decreases with temperature [61–63]. 2,3-Butanedione (diacetyl, Aldrich) was used as a fluorescence xylylene quencher. Other *n*-alcohol (from methanol to hexanol) solvents (Aldrich, spectrophotometric grade or purity >98%) were checked before using.

Experimental details

Steady-state and time-resolved fluorescence measurements were performed by using a SLM 8100C Aminco spectrofluorometer and a Time Correlated Single Photon Counting (TCSPC) FL900 Edinburgh Instruments Spectrometer with a thyratron-gated lamp filled with H_2 respectively. In the latter case the data acquisition was performed with a time window width of 200 ns with a total of 10,000 counts at the intensity maximum. The instrumental response function was obtained from the scattering of a Ludox solution. More details are described elsewhere [58].

Cylindrical quartz 2 mm inner path cells were used for most of the experiments. Corrections due to the inner effect, which are significant at the highest concentrations, were made by the following expression

$$I_{corr} = I_{obs}\, antilog\left(\frac{A_{ex} + A_{em}}{2}\right) \quad (1)$$

where A_{ex} and A_{em} is the absorption at the wavelength of excitation and emission respectively.

Decay intensity profiles were fitted to a sum of exponential decay functions as

$$I(t) = \sum_{i=1}^{n} A_i e^{-t/\tau_i} \quad (2)$$

by the iterative reconvolution method. The intensity weighted average lifetime of a multiple-exponential decay function was then defined as

$$\langle\tau\rangle = \frac{\sum_{i=1}^{n} A_i \tau_i^2}{\sum_{i=1}^{n} A_i \tau_i} \quad (3)$$

where A_i is the pre-exponential factor of the component with a lifetime τ_i of the multi-exponential function intensity decay.

From the fluorescence depolarization measurements, [64] the anisotropy r is defined as:

$$r = (I_{VV} - GI_{VH})/(I_{VV} + 2GI_{VH}) \quad (4)$$

where I_{xy} is the intensity of the emission that is measured when the excitation polarizer is in position x (V for vertical, H for horizontal), the emission polarizer is in position y, and the G factor (= I_{HV}/I_{HH}) corrects for any depolarization produced by the optical system.

For a single excited species which is dynamically quenched, the τ/τ_0 ratio (with/without quencher, Q) is related with [Q] by the linear Stern-Volmer equation. For more complicated systems, the Stern-Volmer representations of $\langle\tau\rangle/\langle\tau_0\rangle$ are only linear at low quencher concentrations [65].

For the dimerization process [58] of X$m\gamma$CD described by the following equilibrium

$$2\,Xm\gamma CD \rightleftarrows (Xm\gamma CD)_2 \quad (5)$$

the association constant K_D expressed as

$$K_D = \frac{[(Xm\gamma CD)_2]}{[Xm\gamma CD]^2} \quad (6)$$

can be related with the fluorescence intensity, I at the maximum of the Xy emission band or measured as are under the emission spectrum, and the total [X$m\gamma$CD] by the equation

$$I = \phi_{(Xm\gamma CD)_2}[Xm\gamma CD] - \left(\phi_{(Xm\gamma CD)_2} - \phi_{Xm\gamma CD}\right) \frac{\left(\sqrt{8K_D[Xm\gamma CD]+1} - 1\right)}{4K_D} \quad (7)$$

where $\phi_{Xm\gamma CD}$ *and* $\phi_{(Xm\gamma CD)_2}$ are the proportionality constants (per chromophore unit) between fluorescence intensity and [X$m\gamma$CD] and [(X$m\gamma$CD)$_2$]. Both parameters are related to their fluorescence quantum yields and molar absorptivities at the excitation wavelength.

On the other hand a non-linear relationship between $\langle\tau\rangle$ and [X$m\gamma$CD] can be obtained as

$$\langle\tau\rangle = \frac{2\tau_{Xm\gamma CD} + \left(\phi_{(Xm\gamma CD)_2}/\phi_{Xm\gamma CD}\right)\tau_{(Xm\gamma 2CD)_2}\left(\sqrt{8K_D[Xm\gamma CD]+1} - 1\right)}{2 + \left(\phi_{(Xm\gamma CD)_2}/\phi_{Xm\gamma CD}\right)\left(\sqrt{8K_D[Xm\gamma CD]+1} - 1\right)} \quad (8)$$

where $\phi_{Xm\gamma CD}$ *and* $\phi_{(Xm\gamma CD)_2}$ are lifetimes for the isolated free and dimer forms. When fluorescence quantum yields for free and dimer forms are similar, $\phi_{(Xm\gamma CD)_2} \approx \phi_{Xm\gamma CD}$, Eq. (7) becomes linear and Eq. (8) is rather simplified.

MM and MD backgrounds

Molecular Mechanics (MM) and Molecular Dynamics (MD) calculations were performed with Sybyl 6.9 [66] and the Tripos Force Field [67]. A relative permittivity ε= 3.5 (ε=1) was used in the vacuum (in the presence of water). Optimizations were carried out by the simplex algorithm, and the conjugate gradient was used as a termination method with gradients of 0.2 (1.0) Kcal/molÅ for the calculations carried out in vacuum (water) [68, 69]. Charges for X$m\gamma$CD in the initial non-distorted conformation (φ=0º and ψ=−3º, τ=115.3° and side chain χ angles in the *trans* conformation [58]) were obtained by MOPAC [70]. Non-bonded cut-off distances were set at 8 Å. The Molecular Silverware algorithm (MS) and periodic boundary conditions (PBC) were used for water solvation [71].

The methods used for the conformational study of the isolated XmCDs and for the dimerization processes were similar to those described previously [58]. In brief the MD

simulations in the vacuo were made in the 300–550 K temperature range at 50 K intervals. The dimerization processes by different head-to-head (*HH*), head-to-tail (*HT*) and tail-to-tail (*TT*), CD-to-CD approaching are depicted in Fig. 1. Critical analysis of the structures generated by scanning the θ [*O(4)-o-o'O(4')*] dihedral angle in the −90 to 90° range (10° intervals) and the *y* coordinate (*oo'* distance) from 20 to 6 Å (1 Å intervals) followed by optimization (PBC, gradient 1 kcal/molÅ) provided the most favorable orientation for approaching which are approximately 30°, 20° and 15° for *HH, HT* and *TT* respectively. Both CDs remain almost parallel to each other. With as initially fixed θ (as Fig. 1 depicts) the 1:1 complexation was emulated by approaching in 0.5 Å steps along the *y* coordinate from 20 to 6 Å. Every step was also optimized in the presence of water and saved for further analysis. Minima binding energy (MBE) for *HH, HT* and *TT* dimeric structures were optimized once again (gradient 0.5 kcal/molÅ) and used as the starting conformations for the 1.0 ns MD simulations following the same strategy described earlier [58]. In a similar way some trimer formation processes were also studied. Starting from the MBE dimer structure the most favorable orientations for the approaching of a third CD were obtained, then the complexation was performed as described for dimers. Trimeric MBE structures were then optimized and 1 ns MD simulation was carried out on them.

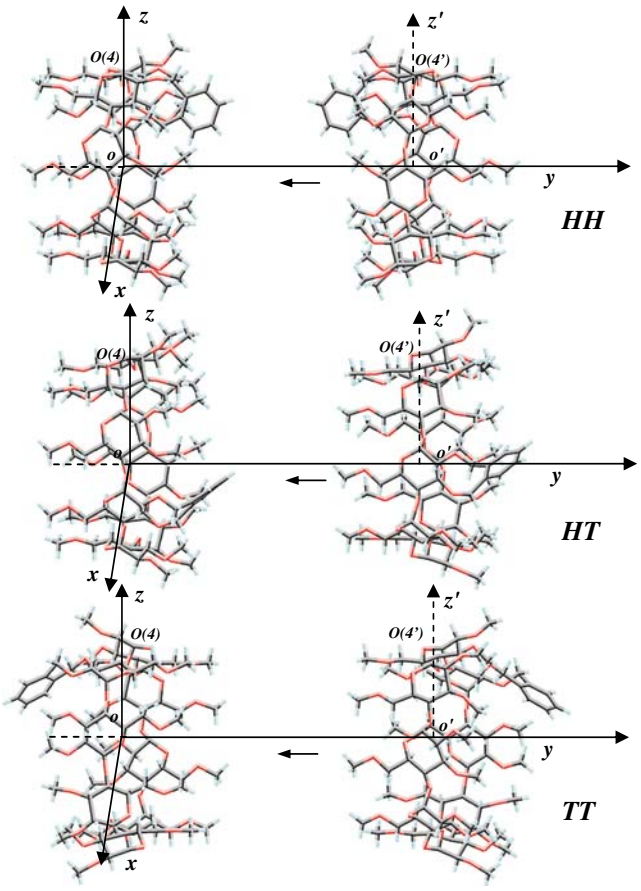

Fig. 1 Coordinate systems used to emulate the dimerization processes by MM with different head-to-head (*HH*), head-to-tail (*HT*) and tail-to-tail (*TT*) X*m*γCDs approaches

Results and discussion

Experimental part

Figure 2 (left) exhibits the fluorescence emission spectra for X*m*γCD water solutions at 25°C obtained upon excitation of the xylylene (Xy) moiety (260 nm). X*m*γCD/water solutions spectra, similarly to *o*Xy, show a single band centered at ~288 nm whose intensity monotonically increases with [X*m*γCD] and decreases with temperature. Whatever the [X*m*γCD] and temperature are, the spectra never point toward the presence of intermolecular Xy excimers.

Figure 2 (right) shows the variation of the corrected (by using Eq. 1) fluorescence intensity measured as the area under the emission spectra with [X*m*γCD] at different temperatures. The representations are nearly linear in the whole range of [X*m*γCD] used in our experiments, which according to Eq. 7 demonstrate that $\phi_{(XmγCD)_2} \approx \phi_{XmγCD}$ i.e., that is, the fluorescence quantum yield for the free X*m*γCD does not change upon dimerization. Obviously this means that fluorescence intensity is not a suitable property to evaluate the association constants for these systems. Something similar occurred with the other X*m*αCD and X*m*βCD members of the series [58].

Fluorescence decay profiles for X*m*γCD/water solutions at different [X*m*γCD] and temperatures were performed at the maximum of the emission of the xylylene band (288 nm) upon 260 nm of excitation. Intensity profiles were fitted to the sum of three-exponential decays with lifetime components in the 0.09–0.24 ns, 3.9–6.4 ns and 6.3–11.6 ns ranges. The fast component, whose contribution decreases with concentration and increases with temperature, was ascribed to the scattering. Most of this contribution is due to the use of cylindrical cells, which exhibit an innate weak scattered light due to stray light. Unfortunately, the low fluorescence quantum yield of Xy ($\Phi_{oXy,water}$=0.029 at 25°C) sometimes makes this component quite important, especially when measuring the lowest concentrations and at the highest temperatures where the fluorescence is thermally quenched. At concentrations slightly higher than the ones used in our measurements, especially at the highest temperatures (these CDs exhibit negative solubility coefficients) where the solubility limit is reached, the intensity profiles show a large component due to the scattering. The middle component, which is attributed to the free unassociated X*m*γCD, shows

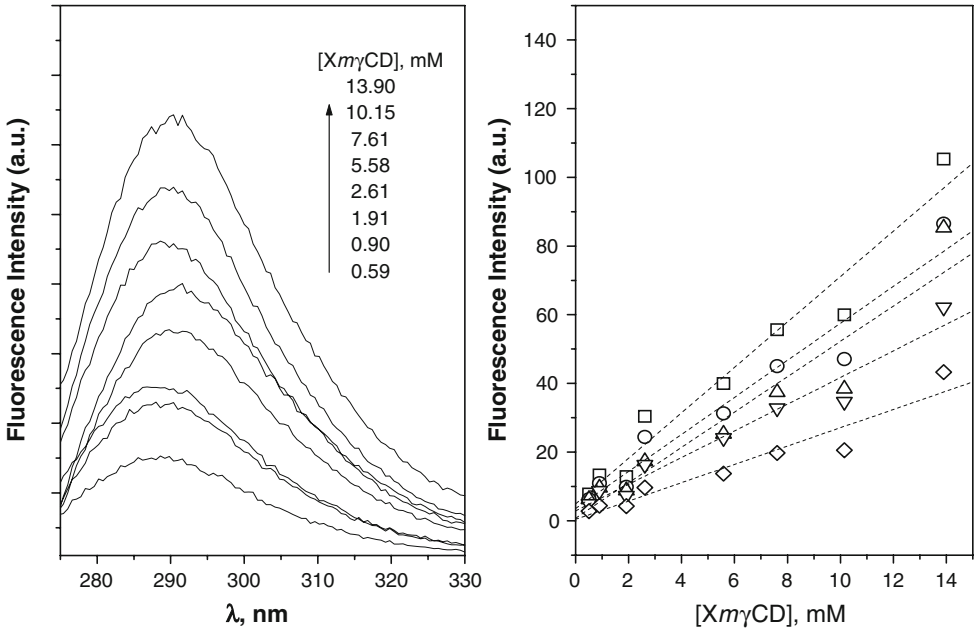

Fig. 2 *left* Emission spectra for X$m\gamma$CD/water solutions of different concentrations at 25°C. *right* Changes of the corrected fluorescence intensity with [X$m\gamma$CD] in the 5–45°C range: 5°C (□); 15°C (○); 25°C (△); 35°C (▽) and 45°C (◊)

values rather similar to those obtained for other member of the series (X$m\alpha$CD and X$m\beta$CD) [58] and its contribution clearly decreases with [XmγCD] and slightly increases with temperature. The slower component, attributed to the presence of dimers, has a value which is considerably smaller than those obtained for the other member of the series [58]. The contribution of this slow component increases with [X$m\gamma$CD] and, in agreement with a possible $\Delta H^0 < 0$ accompanying the association process, decreases with temperature.

Figure 3 depicts the changes in the average lifetime ($\langle\tau\rangle$) obtained by using Eq. 3 with [XmγCD] for X$m\gamma$CD/water solutions at different temperatures. For the calculations of $\langle\tau\rangle$ the component due to the scattering was not taken into account during the fitting process. $\langle\tau\rangle$ increases with [X$m\gamma$CD] since the fraction of associated form, which has a higher lifetime component than the free one, increases. However, as shown in Fig. 3, the magnitude of this increase is considerably smaller than the one obtained for X$m\alpha$CD and X$m\beta$CD systems. The curves correspond to the

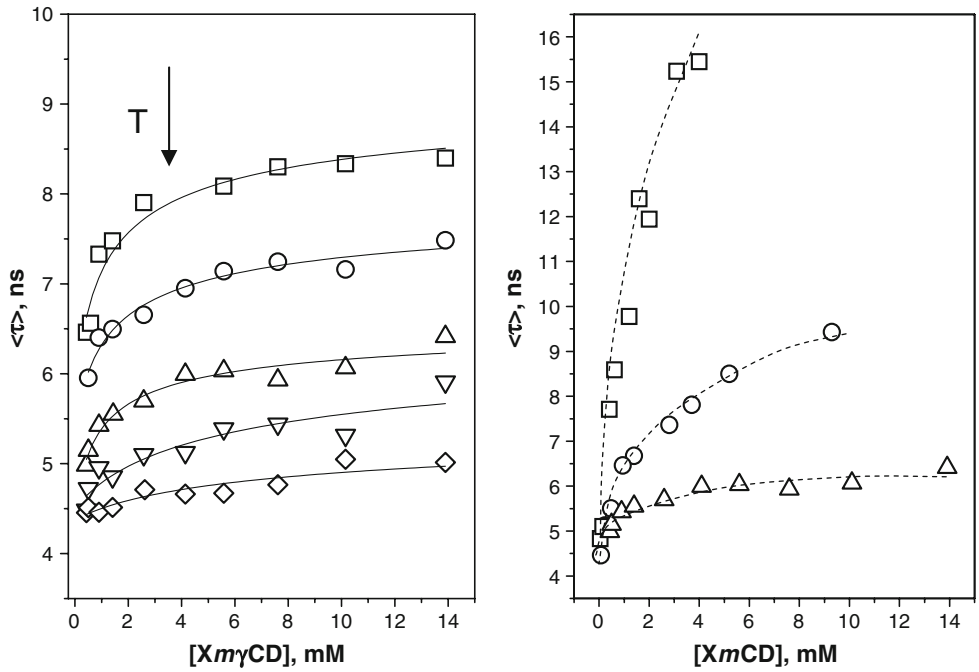

Fig. 3 *left* Variation of the weighted average lifetime $\langle\tau\rangle$ vs [X$m\gamma$CD] at several temperatures: 5°C (□); 15°C (○); 25°C (△); 35°C (▽) and 45°C (◊). *right* $\langle\tau\rangle$ vs [XmCD] for the three X$m\alpha$CD (□), X$m\beta$CD (○) X$m\gamma$CD (△) systems at 25°C (X$m\alpha$CD and X$m\beta$CD data were taken from ref. [58])

adjustments of the experimental data to Eq. 8 on the assumption that $\phi_{(XmγCD)_2}/\phi_{XmγCD} = 1$, thus providing the association constants (K_D), $\tau_{XmγCD}$ *and* $\tau_{(XmγCD)_2}$ values which are collected in Table 1. Although the changes in $\langle\tau\rangle$ with [X*m*γCD] are smaller than those obtained for X*m*αCD and X*m*βCD/water systems, this does not mean that K_D values are smaller. In fact K_D's are slightly larger for X*m*γCD than for the other two members of the series [58]. At the largest [X*m*γCD] (=13.9 mM) used in our experiments, the fraction of X*m*γCD dimerized is relatively low (~0.34). The fact that the xylylene moiety is simultaneously connected to C(2) and C(3) of the glucopyranose unit as a bidentate-hinge by a pair of short chains limits its penetration into the partner CD. According to some authors, this is one of the more plausible reasons for dimer stabilization [20, 23, 25].

ΔH and ΔS values for the association into dimers were obtained from van't Hoff linear representation (Fig. 4) of K_D's at different temperatures and are collected in Table 2. The X*m*γCD dimerization process is accompanied by a highly negative enthalpy change, much larger than the ones obtained for the other members of the series. $\Delta H < 0$ values are usually associated to favorable attractive intermolecular interactions, i.e., van der Waals or hydrogen bonding interactions. The $\Delta S < 0$ values may be due to the loss of rotational and translational degrees of freedom which accompanies any association process, which here is not compensated by entropy gain that would provide the breaking in the water solvating shells of the inner cavity and around a guest when it penetrates inside a CD cavity. This fact suggests that the Xy moiety does not penetrate inside the neighbor X*m*CD cavity, since complexation of small molecules with CDs usually provides $\Delta S > 0$ [5–10].

Fluorescence anisotropy (r), defined by Eq. 4, does not provide much information as the scattering of the sample

Table 1 Association constants K_D, $\tau_{XmγCD}$ *and* $\tau_{(XmγCD)_2}$ parameters obtained from analysis of decay profiles at different [XmγCD] and temperatures

X*m*γCD/water			
T(°C)	K_D(M^{-1})	τ_{XmCD} (ns)	$\tau_{(XmCD)_2}$ (ns)
5	529±135	5.8±1.0	9.3±0.5
15	442±87	5.3±0.5	8.1±0.3
25	(177±80) [a]	(4.3±0.6) [a]	(30.1±4.8) [a]
	(200±74) [b]	(4.4±0.2) [b]	(12.3±0.9) [b]
	248±75	4.8±0.3	7.0±0.4
35	86±50	4.5±0.2	7.1±0.8
45	64±83	4.3±0.1	5.6±0.6

[a] K_D, $\tau_{XmγCD}$ *and* $\tau_{(XmγCD)_2}$ parameters for XmαCD system

[b] *Idem* for XmβCD system. Both data were taken from reference [58]

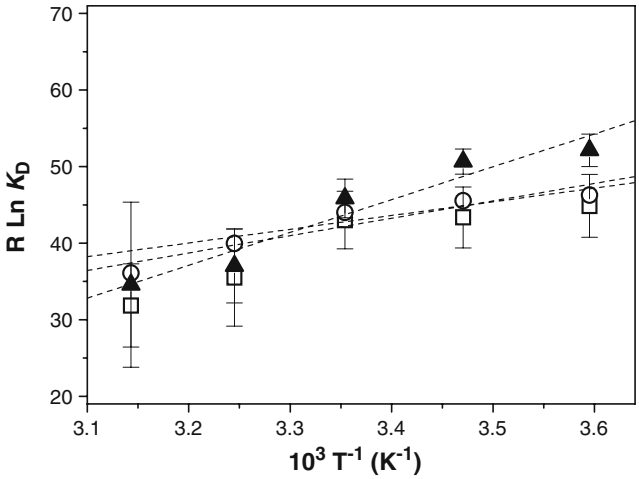

Fig. 4 Van't Hoff representations from the association constants collected in Table 1 for X*m*γCD (▲). Data for X*m*αCD (□) and X*m*βCD (○) systems were also included [58]

makes the interpretation of the results doubtful. In fact, much larger r values than the ones expected for a single appended to CD chromophore in an aqueous medium (r= 0.1130 for [X*m*γCD]=0.5 mM at 25°C), which decrease with [X*m*γCD] (r=0.0118 for [X*m*γCD]=2.61 mM at 25° C) were obtained at the lowest X*m*γCD concentrations (≤ ~2.5 mM). This is due to the high scattering contribution which accompanies the emission at low [X*m*γCD]. However, an increase of r with [X*m*γCD], in agreement with an increase in the dimer fraction, was observed at [X*m*γCD] ≥ ~2.5 mM (r=0.0560 for [X*m*γCD]=13.9 mM at 25°C). The increase of r with temperature (from r=0.0110 at 5°C up to 0.0254 at 45°C for a [X*m*γCD]=2.61 mM) would also agree with the increase in the scattering contribution as the fluorescence intensity is thermally quenched.

Quenching measurements of the xylylene moiety at different temperatures by diacetyl were carried out in a X*m*γCD/water solution at a [X*m*γCD] for which the molar dimer fraction was ~22% as for the previously studied X*m*CD systems [58]. This makes it possible to compare these results with those available for *o*Xy, X*m*αCD and X*m*βCD [58]. Stern-Volmer $\langle\tau\rangle_{q=0}/\langle\tau\rangle$ plots are linear in the range of the quencher concentration ([diacetyl]=0–6×

Table 2 ΔH^0 and ΔS^0 accompanying the dimerization processes of X*m*CD/water systems

System	ΔH (kJmol^{-1})	ΔS (JK^{-1}mol^{-1})
X*m*αCD/water[a]	−29.6±6.9	−60±23
X*m*βCD/water[a]	−22.7±4.4	−34±15
X*m*γCD/water	−100.2±21.8	−43±7

[a] Data from reference 58

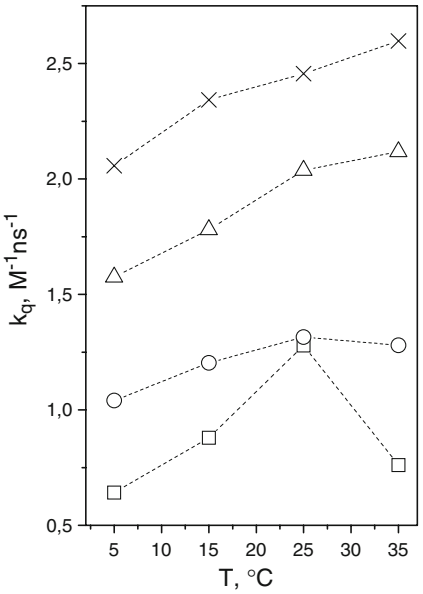

Fig. 5 Variation of the bimolecular quenching constant (k_q) for X*m*αCD (□), X*m*βCD (○), X*m*γCD (△) and *oXy* (×) with temperature. The quencher was diacetyl ($C_4H_6O_2$)

10^{-2}M) used. The bimolecular quenching constants k_q for X*m*γCD exhibit an increase with temperature (Fig. 5), in agreement with the negative ΔH value associated to dimer formation and the larger accessibility to the Xy moiety in the monomer. This result may also be expected for a dynamic quencher process which is controlled by species diffusion and whose efficiency increases when decreasing the viscosity of the milieu with temperature. The results indicate a better exposure of the Xy to the quencher in the o*Xy* than in the X*m*CD/water systems at any temperature. Moreover the access of the quencher to the Xy chromophore in X*m*γCD is rather larger than for the other two X*m*CDs. As the dimer fraction is similar in all experiments, these results could account for different dimer structures formed with the X*m*CDs.

For a better understanding of the fluorescence intensity changes and lifetimes upon dimer formation for X*m*CDs, the dependence of fluorescence quantum yields, Φ, and lifetimes, τ, for *oXy* on the polarity (ε) and microviscosity (η) were studied by measuring the fluorescence properties of *oXy* dilute solutions in different solvents, which cover a wide range of ε and η. All the emission spectra exhibited a single Xy band and the intensity decays were monoexponential for any of the solvents used. As shown in Fig. 6, τ exhibits a decrease with ε and an increase with η. However, Φ hardly depends on ε and η. Dimer formation may involve a decreasing (increasing) in polarity (microviscosity) surrounding the Xy group, as presumably this group may locate itself in a more apolar (and higher microviscosity) environment when X*m*CD associates. As a consequence, the experimental changes in the fluorescence intensity with [X*m*CD] may agree with $\phi_{(XmCD)_2} \approx \phi_{XmCD}$, but also an increase in $\langle\tau\rangle$ (and $\tau_{(XmCD)_2} > \tau_{XmCD}$) may be expected upon dimerization. The amount of the latter variation may be related with the polarity and microviscosity of the X*m*CD cavities or vicinities relative to the corresponding values in water. The fact that $\tau_{(Xm\alpha CD)_2} > \tau_{(Xm\beta CD)_2} > \tau_{(Xm\gamma CD)_2}$ [58] would agree with an increase (decrease) in the polarity (microviscosity) with the X*m*CD macroring size, which is very reasonable. Studies on the complexation of 2-methyl naphthoate, a probe which is sensitive to the medium polarity, reveal that the polarity of natural CD cavities noticeably increases with the size [7].

We have also performed fluorescence measurements on the complexation of *oXy* with *m*γCD and the heterodimerization process between X*m*γCD and *m*γCD in the 5–45°C temperature range. Figure 7 depicts the results obtained from steady-state and time-resolved fluorescence. The non-variation of fluorescence intensity and lifetime averages with [*m*γCD] reveals that X*m*γCD does not form heterodimers with *m*γCD at any temperature. This also occurred for X*m*αCD and X*m*βCD with their corresponding permethylated CDs [58]. The guest *oXy* does not complex with *m*γCD either, as also happened with *m*βCD. The behavior with *m*αCD was different, the *oXy* fitted properly inside the *m*αCD cavity, forming the corresponding 1:1 complex. Nevertheless, this complex exhibited a relatively low binding constant ($K \approx 140$ M^{-1} at 25°C) [58]. These experiments agree with the fact that X*m*γCD dimer formation does not involve the penetration of Xy moiety inside the neighbor CD (quite difficult due to the bidentate-hinge of the xylylene group) and they also support that dimerization may require the presence of two Xy moieties, as heterodimerization with *m*γCD does not take place.

Structures of the isolated X*m*γCD

From the analysis of Molecular Dynamics 1 ns trajectories in the vacuo on X*m*γCD, the probability distribution for φ_i and ψ_i torsional angles of the macroring at different temperatures were obtained. In a way similar to that of other X*m*CDs [58] and natural CDs [72], the ϕ_i and ψ_i angles preferably adopt two skewing conformations from the *trans* state (0°±60°). However, ψ_i can sporadically visit a *cis* state, which is responsible for macroring distortion [72]. The number of visits to this *cis* state increases with temperature. At any temperature the X*m*γCD seems to be more flexible than the other members of the series X*m*α- and X*m*βCDs [58]. As a consequence the number of transits to the different states increases, the population of *cis* states increases and the cavity depth decreases. The distributions of the distances between the center of mass of the benzene ring of the Xy group and the center of mass of

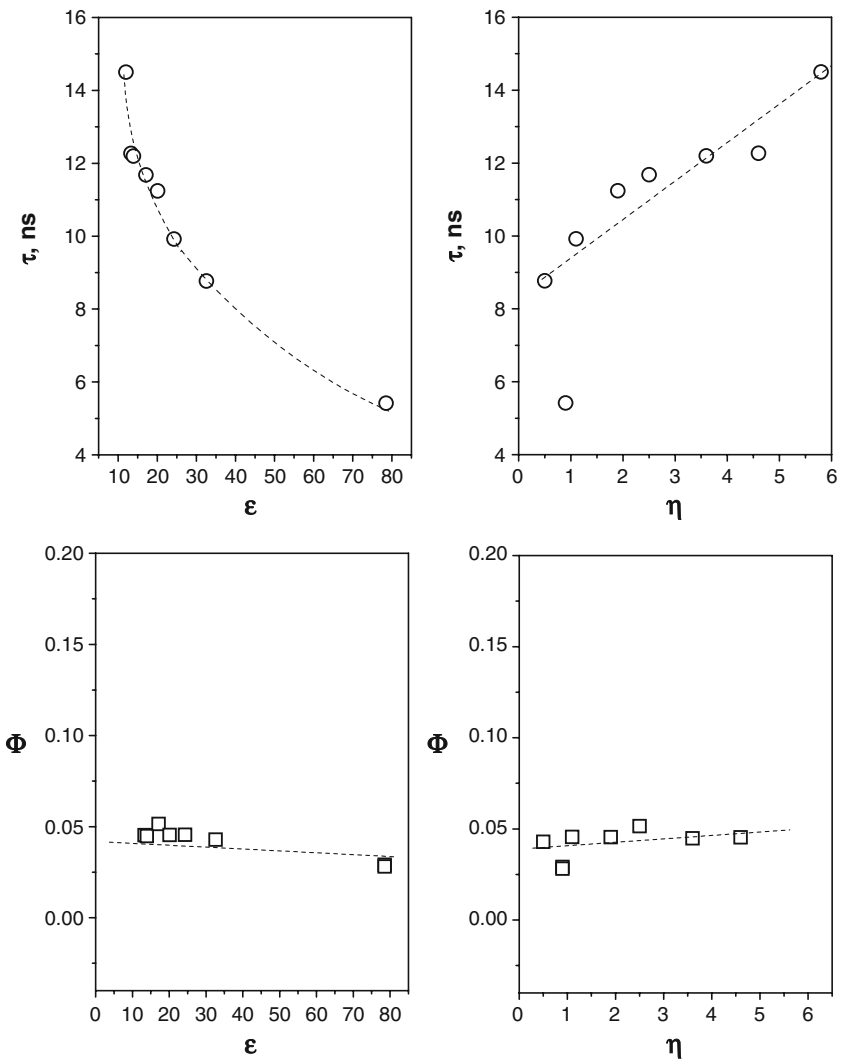

Fig. 6 Variation of the fluorescence quantum yields (Φ) and lifetimes (τ) with the polarity (ε) and microviscosity (η) for *oXy* in different solvents (water and *n*-alcohols from methanol to hexanol) at 25°C

the cyclooligosaccharide moiety (denoted by *o*), depicted in Fig. 8, show a single maxima at any temperature. The average of these distances increases with temperature, this increase being a consequence of the high X*m*γCD macroring flexibility as compared to other member of the series. In addition, these distributions do not show any isosbestic points which may confirm, but not discharge, the presence of an *open/capped* equilibrium, as was previously observed for other members of the series [58]. In the X*m*α- and X*m*βCDs the fraction of molecules that can adopt a *capped* type structure slightly increases with temperature. Now, this equilibrium seems to be markedly displaced toward the *open* form. The analysis also demonstrates the absence of structures where the Xy group is self-included into the cavity. Some of these *capped* and *open* structures are superimposed in Fig. 8. In spite of this flexibility, the torsional angles that describe the rotation around the ether type bonds that connect the appended benzene from the Xy to O2 and O3 of the glucopyranose unit hardly change from the initial position throughout the whole MD trajectory. This indicates that the ϕ_i and ψ_i torsional angles in the macroring are really responsible for the *open/capped* structures.

The whole ensemble of these results, together with the fact that dimerization constants are relatively low, suggests that inclusion processes of an adequate external guest into the isolated X*m*γCD might be feasible, since the entrance to the CD cavity would not be significantly hindered.

Association processes

Figure 9 depicts the changes in the interaction energy for the dimer formation as a function of the distance along the y coordinate (d, Å) between both X*m*γCDs for *HH*, *HT* and *TT* approaches, obtained as described earlier. Although quantitatively different, all three approaches exhibit favorable interactions at the MBE. Most of the MBE, in agreement with $\Delta H < 0$, is due to van der Waals attractive interactions for any of the *HH*, *HT* and *TT* dimers; the

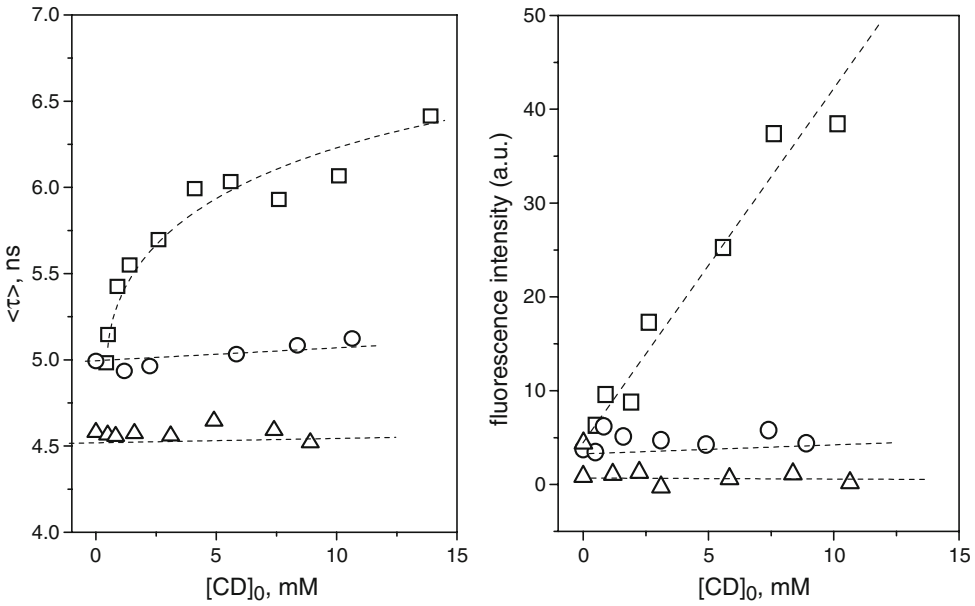

Fig. 7 Changes in the weighted average lifetime $\langle\tau\rangle$ (*left*) and fluorescence intensity relative to the one obtained at the smallest CD concentration (*right*) versus $[CD]_0$ for different systems at 25ºC. Systems are: isolated X*m*γCD (□); *oXy* (< 10^{-5}M, fixed) upon adding *m*γCD (△) and X*m*γCD (0.047 M, fixed) upon adding *m*γCD (○)

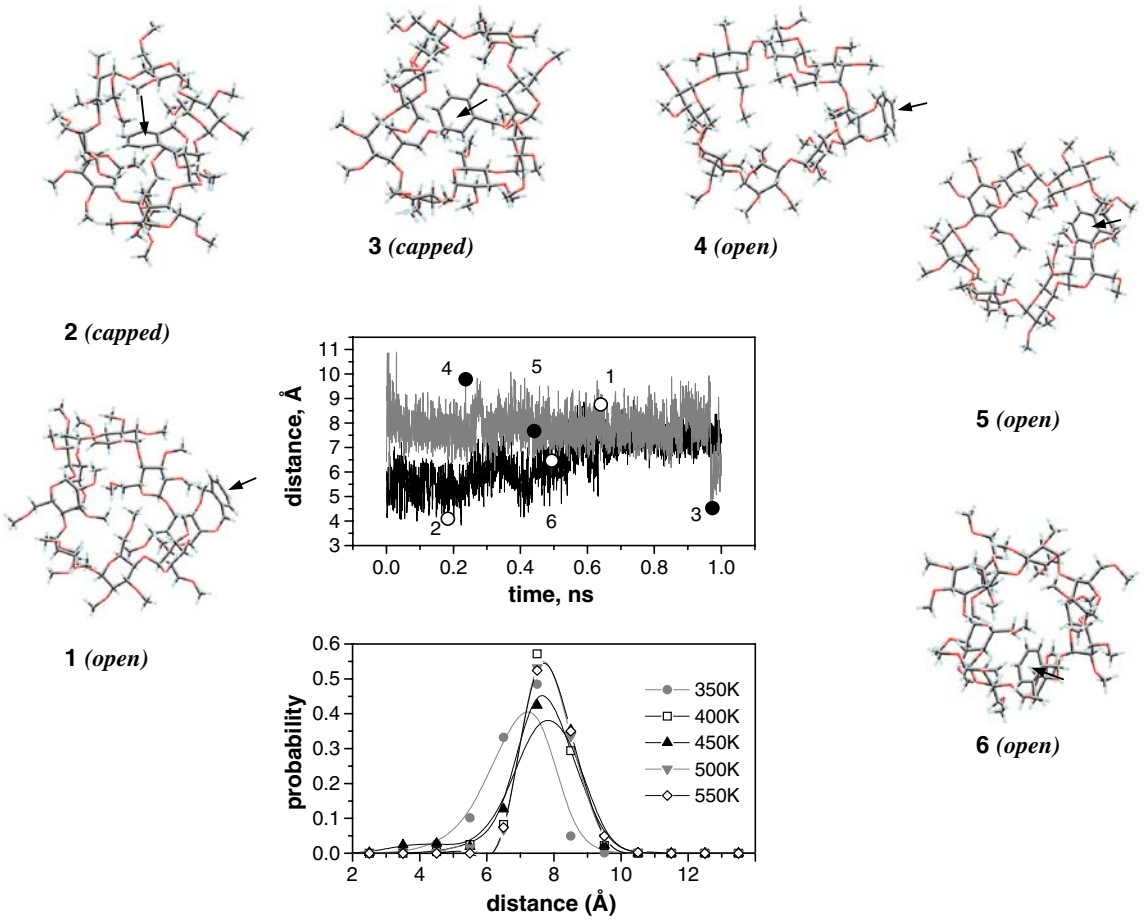

Fig. 8 Histories of the distances (in Å) between the center of masses of benzene from Xy and for CD bridging O atoms for X*m*γCDs at 300 K (*black*) and 500 K (*gray*) (*top panel*). Several *capped-open* conformations obtained from these trajectories were superimposed. Distribution functions for these distances for X*m*γCD at several temperatures (*bottom panel*). Average of the distances (in Å) were 6.9 (0.8); 7.7 (0.7); 7.5 (1.1); 7.8 (0.7) and 7.9 (0.6) at the temperatures shown in the graph. Standard deviations are in parentheses

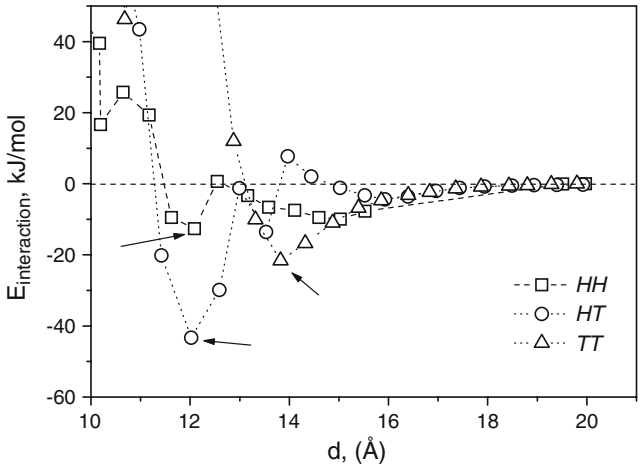

Fig. 9 Changes in the interaction energies when a second X*m*γCD approaches a X*m*γCD (y coordinate in Å) by *HH* (□), *HT* (○) and *TT* (△) orientations. Arrows point out the MBE $(Xm\gamma CD)_2$ structures whose geometrical and energetic parameters are collected in Table 3

electrostatic interactions, mostly unfavorable, however, are much less significant at any distance. Table 3 collects some geometrical parameters and different interaction energy contributions that involve the Xy moieties of X*m*γCDs. The Xy-Xy interactions, due to the short Xy-Xy distance, seem to be unfavorable for the MBE *HH* dimer (for other approaches this interaction does obviously not exist). At this X*m*γCD distance, only one of the Xy groups favorably interacts with the partner CD macroring.

Figure 10 (left) shows the MBE structures for the *HH* and *HT* $(Xm\gamma CD)_2$ dimers that, once optimized (0.5 kcal/Åmol), were used as starting structures for MD simulations. For both structures the Xy groups adopt an *open* conformation.

Figure 11 shows the history of the interaction energies and some contributions where the Xy group is involved obtained from the analysis of the 1.0 ns MD trajectories for the *HH*, *HT* and *TT* $(Xm\gamma CD)_2$ structures. Table 4 collects the values of some of the parameters obtained for the minima binding energy structure obtained from the analysis of these trajectories. As for $(Xm\alpha CD)_2$ and $(Xm\beta CD)_2$, the *HH* $(Xm\gamma CD)_2$ seems to be energetically more favorable than those obtained when X*m*CDs approach by any other orientation. Nevertheless, *HT-type* dimers also show important favorable interaction energy along most of the trajectory, but it dissociates at the last part of the trajectory. *TT-type* dimer disappears quite fast. An *HH-type* dimer would agree with the fact that experimentally $(Xm\gamma CD)_2$ dimers are spontaneously formed in X*m*γCD/water solutions, but X*m*γCD-*m*γCD heterodimers are not. However, *HT-type* dimers would agree with the quenching experiments and a relatively high Xy group accessibility in the $(Xm\gamma CD)_2$ dimers, as compared to the analogous $(Xm\alpha CD)_2$ and $(Xm\beta CD)_2$. As collected in Table 4, the interaction energies for the MBE structures where Xy groups are involved, when they exist, were always favorable whatever the *HH* or *HT* approach was. This probably means that both *HH*- or *HT*-types would be possible. Figure 12 (right) depicts MBE structures for both types of dimers obtained from analysis of the 1.0 ns MD trajectories.

Accepting the presence of *HT*-type dimer structures and considering the possibility of larger order *HT n*-mer formation, a new X*m*γCD was approached to the MBE *HT*-type dimer obtained from the MM calculation. The procedure was similar to the one described for the dimer formations. The MBE *HT* trimer structure was optimized and a 1 ns MD trajectory was simulated.

Figure 12 depicts the histories for the distances and some interaction energies between pairs of neighbor X*m*γCDs in the trimer (1–2 and 2–3). Interaction energies between 1

Table 3 Binding energy and some energy contribution energies ($kJmol^{-1}$) for the structures of MBE (*min*) and at the largest X*m*CD- X*m*CD separation (∞) for X*m*γCD by *HH*, *HT* and *TT* approaching. ε remains nearly close to 90°

Parameter	HH_{min}	HH_{∞}	HT_{min}	HT_{∞}	TT_{min}	TT_{∞}
Distance (Å)	12.1	20.0	12.0	19.9	13.8	19.8
Distance Xy1-Xy2 (Å)	4.5	9.3	12.3	20.2	24.6	30.6
θ (°)	30.2	30.3	18.8	18.6	13.8	90.9
$E_{binding}$ (kJ/mol)	−12.6	−0.0	−43.3	−0.0	−21.6	0
electrostatics	3,9	0.2	2.0	0.0	6.0	−0.0
van der Waals	−16.5	−0.2	−45.3	−0.0	−27.6	0
E_{inter} Xy2-X*m*CD1	9.2	−0.0	−11.6	−0.0	0	0
electrostatics	1.2	0.2	−5.4	0.0	0	−0.0
van der Waals	8,0	−0.2	−6.2	−0.0	−0.0	0
E_{inter} Xy1-X*m*CD2	−5.5	−0.0	0	0	0.0	0
electrostatics	2.6	0.2	0	0.0	0	0
van der Waals	−8.1	−0.2	−0.0	0	0.0	0
E_{inter} Xy1-Xy2	5.0	−0.0	0	−0.0	0.0	0
electrostatics	5.1	0.2	0	0	0	0
van der Waals	−0.0	−0.2	−0.0	0.0	−0.0	0

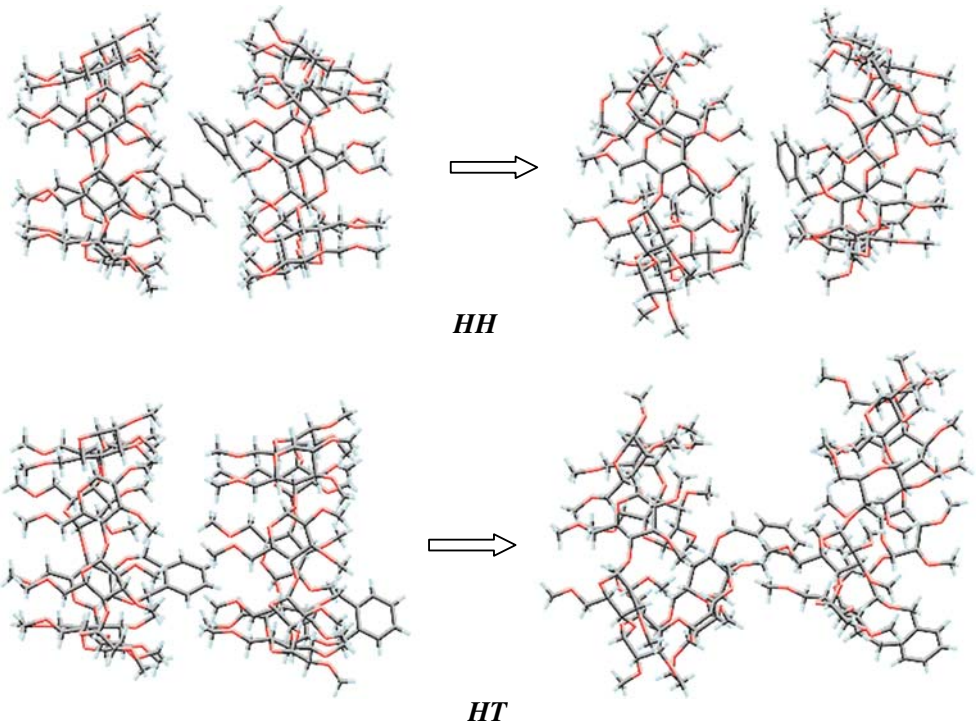

Fig. 10 MBE *HH-type* (*upper*) and *HT-type* (*bottom*) $(XmγCD)_2$ structures obtained from MM (*left*) and MD trajectory analysis (*right*)

and 2 X*m*γCDs are favorable throughout the whole trajectory, however, after one third of the trajectory the third X*m*γCD hardly interacts with the one adjacent to it. Apparently dimers are stable but the addition of a third X*m*γCD does not stabilize the system.

Conclusions

Steady-state and time-resolved fluorescence techniques and Molecular Modeling were employed to study the self-association in water of $2^{I},3^{I}$-*O*-(*o*-xylylene)-per-*O*-

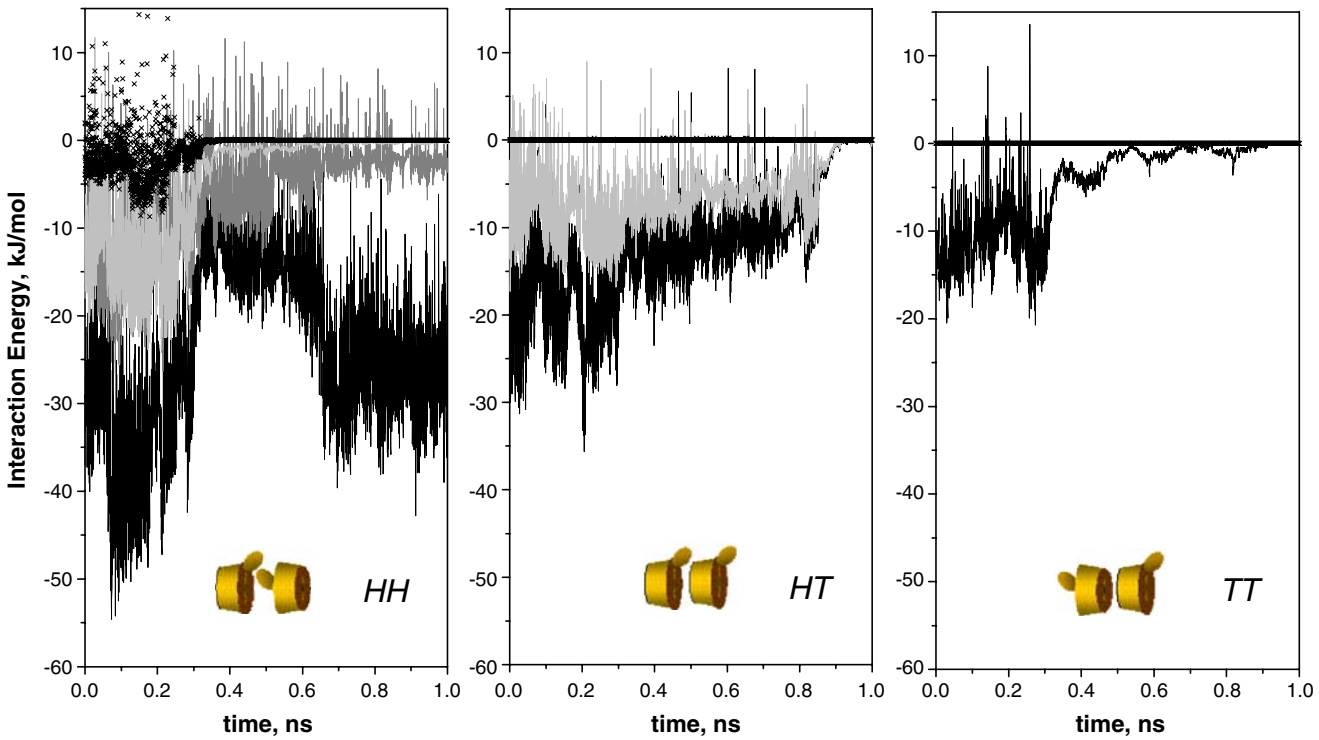

Fig. 11 Histories of different interaction energies for *HH*-, *HT*- and *TT*-type $(XmγCD)_2$ dimers obtained from 1 ns MD trajectories at 300 K: Interaction energies are: X*m*γCD-X*m*γCD (*black*), Xy(1)-X*m*γCD(2) (*light gray*), Xy(2)-X*m*γCD(1) (*gray*) and Xy(1)-Xy(2) (*black symbols*)

Table 4 Binding energy and some other interaction energy contribution ($kJmol^{-1}$) for the structures of MBE for X*m*γCD by *HH*, *HT* and *TT* approaching obtained after the analysis of MD 1.0 ns trajectories

Parameter	*HH*	*HT*	*TT*
Distance (Å)	12.4	14.2	15.1
Distance Xy1-Xy2 (Å)	5.8	12.3	27.0
θ (°)	45.7	7.1	−23.1
ε (°)	78.5	80.8	116.0
$E_{binding}$ (kJ/mol)	−54.6	−35.6	−20.7
electrostatics	−0.6	−5.3	0.1
van der Waals	−53.9	−30.3	−20.7
E_{inter} Xy2-XmCD1	−25.3	−11.5	0
E_{inter} Xy1-XmCD2	−20.4	0	0
E_{inter} Xy1-Xy2	−4.9	0	0

Me-γ-cyclodextrin (XmγCD). Lifetime averages $\langle\tau\rangle$ obtained from analysis of decay profiles for XmγCD/water solutions at different temperatures allowed us to obtain dimerization equilibrium constants, K_D, and thermodynamics parameters during association. The process was enthalpically governed and entropically disfavoured, as it was the case for the X*m*αCD and X*m*βCD previously studied. The $\Delta H < 0$ values were typical of attractive van der Waals interactions, whereas the $\Delta S < 0$ values corresponded to the loss of freedom degrees during association. MD simulations, performed to study the conformational behaviour of isolated XmγCD in the vacuo at different temperatures, demonstrated the presence of an *open* ⇄ *capped* equilibrium which was displaced to the *open* conformation. Rotation around the bonds at the brindging oxygen atoms of the CD macroring seems to be responsible for these two arrangements. Simulations of the dimerization processes in water showed that $(Xm\gamma CD)_2$ dimers can preferably be formed by head-to-head CD approaching. However, in agreement with quenching measurements, the formation of stable head-to-tail dimers is not dismissed.

Acknowledgments This work was supported by the Spanish MEC (projects CTQ2006-15515C02-01/BQU, CTQ2007-61180/PPQ,

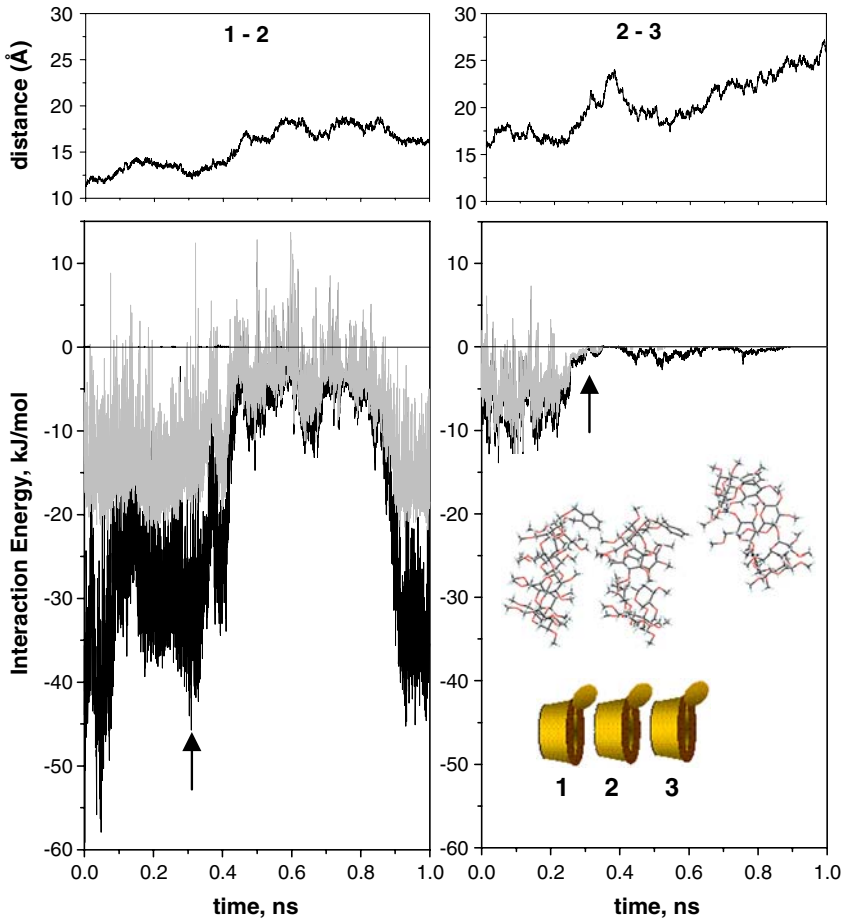

Fig. 12 Histories of interaction energies for *HT*-type $(Xm\gamma CD)_3$ trimer obtained from the 1 ns MD trajectory at 300 K. Interaction energies are (*left*): X*m*γCD(1)-X*m*γCD(2) (*black*), Xy1-X*m*γCD2 (*light gray*); (*right*) X*m*γCD(2)-X*m*γCD(3) (*black*) and Xy2-X*m*γCD3 (*light gray*); Other Xy-X*m*γCD or Xy-Xy interactions are obviously negligible

CTQ2005-04710/BQU and CTQ2008-03149/BQU), the Junta de Andalucía (P06-FQM-01601), the Comunidad de Madrid (S-055/MAT/0227) and the Junta de Castilla-La Mancha (grant to M.J.G-A). FM and MJG-A acknowledge the assistance of M. L. Heijnen with the preparation of the manuscript and L. M. Frutos for his valuable co-operation in some calculations.

References

1. Szejtli J, Osa T (1996) Comprehensive supramolecular chemistry, Vol. 3. Pergamon, Oxford
2. D'Souza VT, Lipkowitz KB (1998) Cyclodextrins: introduction. Chem Rev 98(5):1741–1742. doi:10.1021/cr980027p
3. Harada A (2001) Cyclodextrin-based molecular machines *A*. Acc Chem Res 34(6):456–464. doi:10.1021/ar000174l
4. Nepogodiev SA, Stoddart JF (1998) Cyclodextrin-based catenanes and rotaxanes. Chem Rev 98(5):1959–1976. doi:10.1021/cr970049w
5. Madrid JM et al (1999) Experimental thermodynamics and molecular mechanics calculations of inclusion complexes of 9-methyl anthracenoate and 1-methyl pyrenoate with β-cyclodextrin. J Phys Chem B 103(23):4847–4853. doi:10.1021/jp9838240
6. Cervero M, Mendicuti F (2000) Inclusion complexes of dimethyl 2, 6-naphthalenedicarboxylate with α- and β-cyclodextrins in aqueous medium: thermodynamics and molecular mechanics studies. J Phys Chem B 104(7):1572–1580. doi:10.1021/jp993418w
7. Di Marino A, Mendicuti F (2002) Fluorescence of the complexes of 2-methylnaphthoate and 2-hydroxypropyl-α-, -β-, and -γ-cyclodextrins in aqueous solution. Appl Spectrosc 56(12):1579–1587. doi:10.1366/000370202321115841
8. Pastor I, Di Marino A, Mendicuti F (2005) Complexes of dihexyl 2, 6-naphthalenedicarboxylate with α- and β-cyclodextrins: fluorescence and molecular modelling. J Photochem Photobiol 173(3):238–247. doi:10.1016/j.jphotochem.2005.04.003
9. Di Marino A, Rubio L, Mendicuti F (2007) Fluorescence and molecular mechanics of 1-methyl naphthalenecarboxylate/cyclodextrin complexes in aqueous medium. J Incl Phenom Macrocycl Chem 58(1–2):103–114. doi:10.1007/s10847-006-9129-7
10. Alvariza C et al (2007) Binding of dimethyl 2,3-naphthalenedicarboxylate with α-, β- and γ-cyclodextrins in aqueous solution. Spectroc Acta Pt A Mol Biomolec Spectr 67A(2):420. doi:10.1016/j.saa.2006.07.039
11. Kodaka M, Fukaya T (1989) Induced circular dichroism spectrum of a α-cyclodextrin complex with heptylviologen. Bull Chem Soc Jpn 62(4):1154–1157. doi:10.1246/bcsj.62.1154
12. Ueno A et al (1990) Host-guest sensory system of dansyl-modified β-cyclodextrin for detecting steroidal compounds by dansyl fluorescence. Chem Lett 4:605–608. doi:10.1246/cl.1990.605
13. Berberan-Santos MN et al (1992) Multichromophoric cyclodextrins.1. Synthesis of o-naphthoyl-β-cyclodextrins and investigation of excimer formation and energy hopping. J Am Chem Soc 114(16):6427–6436. doi:10.1021/ja00042a021
14. Berberan-Santos MN et al (1993) Multichromophoric cyclodextrins.2. Inhomogeneous spectral broadening and directed energy hopping. J Phys Chem 97(44):11376–11379. doi:10.1021/j100146a006
15. Kodaka M (1993) A general rule for circular dichroism induced by a chiral macrocycle. J Am Chem Soc 115(9):3702–3705. doi:10.1021/ja00062a040
16. Hamasaki K et al (1993) Fluorescent sensors of molecular recognition. Modified cyclodextrins capable of exhibiting guest-responsive twisted intramolecular charge transfer fluorescence. J Am Chem Soc 115(12):5035–5040. doi:10.1021/ja00065a012
17. Gravett DM, Guillet JE (1993) Synthesis and photophysics of a water-soluble, naphthalene-containing β-cyclodextrin. J Am Chem Soc 115(14):5970–5974. doi:10.1021/ja00067a011
18. Jullien L et al (1994) Antenna effect in multichromophoric cyclodextrins. Angew Chem Int Ed Engl 106(23/24):2582–2584
19. Wang Y et al (1994) Dansyl-β-cyclodextrins as fluorescent sensors responsive to organic compounds. Bull Chem Soc Jpn 67(6):1598–1607. doi:10.1246/bcsj.67.1598
20. McAlpine SR, Garcia-Garibay MA (1996) Inside–outside isomerism of β-cyclodextrin covalently linked with a naphthyl group. J Am Chem Soc 118(11):2750–2751. doi:10.1021/ja953061j
21. Park JW, Choi NH, Kim JH (1996) Facile dimerization of viologen radical cations covalently bonded to β-cyclodextrin and suppression of the dimerization by β-cyclodextrin and amphiphiles. J Phys Chem 100(2):769–774. doi:10.1021/jp9520308
22. Ikeda H (1996) Fluorescent cyclodextrins for molecule sensing: fluorescent properties, NMR characterization, and inclusion phenomena of N-dansylleucine-modified cyclodextrins. J Am Chem Soc 118(45):10980–10988. doi:10.1021/ja960183i
23. McAlpine SR, García-Garibay MA (1996) Binding studies of adamantanecarboxylic acid and a naphthyl-bound β-cyclodextrin by variable temperature 1H NMR. J Org Chem 61(23):8307–8309. doi:10.1021/jo9613794
24. Ikeda H et al (1997) NMR studies of conformations of N-dansyl-L-leucine-appended and N-dansyl-D-leucine-appended β-cyclodextrin as fluorescent indicators for molecular recognition. J Org Chem 62(5):1411–1418. doi:10.1021/jo960425x
25. McAlpine SR, Garcia-Garibay MA (1998) Studies of naphthyl-substituted β-cyclodextrins. Self-aggregation and inclusion of external guests. J Am Chem Soc 120(18):4269–4275. doi:10.1021/ja972810p
26. Schneider H-J, Hacket F, Rüdiger V (1998) NMR studies of cyclodextrins and cyclodextrin complexes. Chem Rev 98 (5):1755–1785. doi:10.1021/cr970019t
27. Ishizu T, Kintsu K, Yamamoto H (1999) NMR study of the solution structures of the inclusion complexes of β-cyclodextrin with (+)-catechin and (−)-epicatechin. J Phys Chem B 103 (42):8992–8997. doi:10.1021/jp991178e
28. Ikunaga T et al (1999) The effects of avidin on inclusion phenomena and fluorescent properties of biotin-appended dansyl-modified β-cyclodextrin. Chem Eur J 5(9):2698–2704. doi:10.1002/(SICI)1521-3765(19990903)5:9<2698::AID-CHEM2698>3.0.CO;2-G
29. Berberan-Santos MN et al (1999a) Multichromophoric cyclodextrins.6. Investigation of excitation energy hopping by Monte-Carlo simulations and time-resolved fluorescence anisotropy. J Am Chem Soc 121(11):2526–2533. doi:10.1021/ja983601n
30. Berberan-Santos MN et al (1999b) Multichromophoric cyclodextrins. 8. Dynamics of homo- and heterotransfer of excitation energy in inclusion complexes with fluorescent dyes. J Am Chem Soc 122(48):11876–11886. doi:10.1021/ja000995l
31. Hoshino T et al (2000) Daisy chain necklace: tri[2]rotaxane containing cyclodextrins. J Am Chem Soc 122(40):9876–9877. doi:10.1021/ja0018264
32. Fujimoto T et al (2000) The first lipophilic face-to-face dimers of permethylated α-cyclodextrin-azobenzene dyads through a p-xylylene spacer. Chem Lett 5:564–565. doi:10.1246/cl.2000.564
33. Fujimoto T (2000) The first lipophilic face-to-face dimers of permethylated α-cyclodextrin-azobenzene dyads through a p-xylylene spacer. Chem Lett 7:764–765. doi:10.1246/cl.2000.764
34. Mirzoian A, Kaifer AE (1999) Electrochemically controlled self-complexation of cyclodextrin-viologen conjugates. Chem Commun (Camb) 16:1603–1604. doi:10.1039/a904095a
35. Liu Y et al (2000) Molecular Interpenetration within the columnar structure of crystalline anilino-β-cyclodextrin. Org Lett 2:2761–2763. doi:10.1021/ol000135+
36. Inoue Y et al (2000) Supramolecular photochirogenesis.2.Enantiodifferentiating photoisomerization of cyclooctene included and sensitized by 6-O-modified cyclodextrins. J Org Chem 65 (23):8041–8050. doi:10.1021/jo001262m

37. Fujimoto T et al (2001) Photoswitching of the association of a permethylated α-cyclodextrin-azobenzene dyad forming a Janus [2]pseudorotaxane. Tetrahedron Lett 42(45):7987–7989. doi:10.1016/S0040-4039(01)01563-5
38. Aoyagi T et al (2001) Fluorescence properties, induced-fit guest binding and molecular recognition abilities of modified γ-cyclodextrins bearing two pyrene moieties. Bull Chem Soc Jpn 74(1):157–164. doi:10.1246/bcsj.74.157
39. Park K (2001) Preparation and self-inclusion properties of p-xylylenediamine-modified β-cyclodextrins: dependence on the side of modification. J Chem Soc Perkin Trans 2(11):2114–2118. doi:10.1039/b105388b
40. Kuwabara T et al (2002) Hetero-dimerization of dye-modified cyclodextrins with native cyclodextrins. J Org Chem 67(3):720–725. doi:10.1021/jo010696u
41. Park JW et al (2002) Facile dimerization and circular dichroism characteristics of 6-O-(2-Sulfonato-6-naphthyl)-β-cyclodextrin. J Phys Chem B 106(20):5177–5183. doi:10.1021/jp014191j
42. Park JW et al (2002) Face selectivity of inclusion complexation of viologens with β-cyclodextrin and 6-O-(2-sulfonato-6-naphthyl)-β-cyclodextrin. J Phys Chem B 106(29):7186–7192. doi:10.1021/jp020428f
43. Harada A et al (2003) Supramolecular polymers formed by cinnamoyl cyclodextrins. J Polym Sci A Polymer Chem (Kyoto) 41(22):3519–3523
44. Liu Y et al (2003) Supra-molecular self-assemblies of β-cyclodextrins with aromatic tethers: factors governing the helical columnar versus linear channel super-structures. Org Chem 68 (22):8345–8352. doi:10.1021/jo034632q
45. Park JW et al (2003) Homo-dimerization and hetero-association of 6-O-(2-sulfonato-6-naphthyl)-γ-cyclodextrin and 6-deoxy-(pyrene-1-carboxamido)-β-cyclodextrin. J Org Chem 68(18):7071–7076. doi:10.1021/jo034623h
46. Liu Y et al (2003) Binding ability and self-assembly behavior of linear polymeric supramolecules formed by modified β-cyclodextrin. Org Lett 5(3):251–254. doi:10.1021/ol027146i
47. Balzani V (2003) Molecular devices and machines: a journey into the Nanoworld. Wiley-VCH, Weinhein
48. Miyauchi M et al (2005) A [2]Rotaxane capped by a cyclodextrin and a guest: formation of supramolecular [2]Rotaxane polymer. J Am Chem Soc 127(7):2034–2035. doi:10.1021/ja042840+
49. Miyauchi M, Harada A (2005) A helical supramolecular polymer formed by host–guest interactions. Chem Lett 34(1):104–105. doi:10.1246/cl.2005.104
50. Miyauchi M et al (2005) Chiral supramolecular polymers formed by host–guest interactions. J Am Chem Soc 127(9):2984–2989. doi:10.1021/ja043289j
51. Hasewaga Y et al (2005) Supramolecular polymers formed from βciclodextrins dimer linked by poly(ethyleneglycol) and guest dimers. Macromolecules 38(9):3724–3730. doi:10.1021/ma047451e
52. Park JW (2005) Efficient inclusion complexation and intra-complex excitation energy transfer between aromatic group-modified β-cyclodextrins and a hemicyanine dye. J Photochem Photobiol Chem 173(3):271–278. doi:10.1016/j.jphotochem.2005.04.006
53. Ikeda H et al (2005) Skeleton-selective fluorescent chemosensor based on cyclodextrin bearing a 4-amino-7-nitrobenz-2-oxa-1, 3-diazole moiety. Org Biomol Chem 3(23):4262–4267. doi:10.1039/b508477f
54. Nakashima H, Yoshida N (2006) Fluorescent detection for cyclic and acyclic alcohol guests by naphthalene-appended amino-β-cyclodextrins. Org Lett 8(22):4997–5000. doi:10.1021/ol0616079
55. Wu A et al (2006) Investigation on photophysical properties of a substituted 3H-indole-modified β-cyclodextrin. J Photochem Photobiol Chem 182(2):174–180. doi:10.1016/j.jphotochem. 2006.02.008
56. González-Álvarez MJ et al (2008) Study of the conformational and self-aggregation properties of 2I, 3I-O-(o-Xylylene)-per-O-Me-α- and -β-cyclodextrins by fluorescence and molecular modeling. J Chem Phys 112:13717–13729
57. Engeldinger E et al (2003) Capped cyclodextrins. Chem Rev 103 (11):4147–4173. doi:10.1021/cr030670y
58. Balbuena P et al (2007) One-pot regioselective synthesis of 2I,3I-O-(o-xylylene)-capped cyclomaltooligosaccharides: tailoring the topology and supramolecular properties of cyclodextrins. Chem Commun (Camb) 31:3270–3272 doi:10.1039/b705644c
59. Wang W (1997) Synthetic study of selective benzylic oxidation. J Org Chem 62(19):6598–6602. doi:10.1021/jo962172d
60. Uekama K, Irie T (1987) Cyclodextrins and their industrial uses. D.Duchême Edition Sante, Paris, Chapter 10
61. Aree T et al (2000) Novel type of thermostable channel clathrate hydrate formed by heptakis(2, 6-di-O-methyl)-β-cyclodextrin·15H2O-a paradigm of the hydrophobic effect. Angew Chem Int Ed 39(5):897–899. doi:10.1002/(SICI)1521-3773(20000303)39:5<897::AID-ANIE897>3.0.CO;2-R
62. Jefrey GA (1996) In: Atwood JL, Davies JED, MacNicol DD, Vögtle F (eds) Comprehensive supramolecular chemistry, Vol. 6, Chap. 23. Pergamon Press, Oxford
63. Starikov EB et al (2001) Negative solubility coefficient of methylated cyclodextrins in water: a theoretical study. Chem Phys Lett 336:504–510. doi:10.1016/S0009-2614(01)00160-9
64. Lakowicz JR (1999a) Principles of fluorescence spectroscopy, 2nd edn. Kluwer, New York, p 298
65. Lakowicz JR (1999b) Principles of fluorescence spectroscopy, 2nd edn. Kluwer, New York, p 239
66. SYBYL molecular modeling software (Version 6.9), Tripos Associates, Inc., St. Louis, MO
67. Clark M et al (1989) Validation of the general purpose Tripos 5.2 force field. J Comput Chem 10(8):982–1012. doi:10.1002/jcc.540100804
68. Brunel Y et al (1975) Program of minimization of the empirical energy of a molecule by a simple method. Tetrahedron 31 (8):1075–1091. doi:10.1016/0040-4020(75)80129-3
69. Press W et al (1988) Numerical recipes: the art of scientific computing. Cambridge University Press, Cambridge, p 312
70. Frisch MJ et al (2004) MOPAC (AM1): included in the Gaussian 03 package. Gaussian 03, revision C.02. Gaussian, Wallingford, CT
71. Blanco M (1991) Molecular silverware. I. General solutions to excluded volume constrained problems. J Comput Chem 12 (2):237–247. doi:10.1002/jcc.540120214
72. Pozuelo J et al (1996) Inclusion complexes of chain molecules with cycloamyloses. 1. Conformational analysis of the isolated cycloamyloses using molecular dynamics simulations. Comput Theor Polym Sci 6:125–134